Reusable melanin-based biosorbents for efficient methylene blue removal: the new frontier of fungi-inspired allomelanin coatings for sustainable water remediation processes

Valeria Lino[a,b†], Rachele Castaldo[c†], Gennaro Gentile[c]*, Paola Manini[b]*

[a]Scuola Normale Superiore, Piazza dei Cavalieri 7, I-56126 Pisa, Italy. valeria.lino@sns.it

[b]Department of Chemical Sciences, University of Napoli Federico II, Complesso Universitario Monte S. Angelo, via Cintia 4, I-80126 Napoli, Italy. pmanini@unina.it

[c]Institute for Polymers Composites and Biomaterials, National Research Council of Italy, Via Campi Flegrei 34, 80078 Pozzuoli, Italy. gennaro.gentile@cnr.it, rachele.castaldo@ipcn.cnr.it

*Corresponding authors

Prof. Paola Manini, e-mail address: pmanini@unina.it

Dr Gennaro Gentile, e-mail address: gennaro.gentile@cnr.it

Materials Today Sustainability
Volume 21, March 2023, 100283
https://doi.org/10.1016/j.mtsust.2022.100283

Abstract

The impact of water pollution caused by industrial wastes on our society prompted the urgent search for efficient remediation processes. Moved by the increasing interest in this research field, we report herein on the design and fabrication of an innovative water filtering device based on a nylon membrane coated with a synthetic melanin polymer inspired by fungal allomelanins and generated via the oxidative polymerization of 1,8-dihydroxynaphthalene.

The melanin coating, obtained via the straightforward and low-cost ammonia induced solid state polymerization technique, proved to be highly stable with no evidence of debonding phenomena, did not alter the porous structure of the nylon filter and its flow rate and induced a slight but appreciable improvement of its tensile properties.

The adsorbing performances of the melanin coated membrane were tested toward the azo dye methylene blue both in batch and in-flow conditions and compared with those of the synthetic melanin polymer as a bulk. The data revealed that the adsorption process: a) fits quite well with the Langmuir isotherm model, suggesting a monolayer adsorption on a surface with homogeneous sites, with a maximum adsorption capacity of 262 mg/g; b) is a favourable, exothermic and spontaneous process; c) is governed by a pseudo-second order kinetics.

The in-flow experiments revealed the high efficiency of the filtering membrane in removing MB up to 99%; moreover, tests carried out to assess the regeneration and reuse of the membrane showed that the methylene blue removal efficiency was not affected up to seven adsorbing/desorbing cycles.

Keywords

Fungal melanin nanoparticles, microporous organic polymer, water remediation, water filtering membrane, methylene blue adsorption, biosorbent

1. Introduction

Nowadays, the high levels of water pollution determined by the discharge of industrial effluents and the lack of safe drinking water supply have stimulated the research for always more effective water remediation processes [1-3]. In this regard, different strategies have been pursued based on physical, chemical, electrochemical and biological approaches, such as solvent extraction, micro and ultrafiltration, advanced oxidation processes, ion exchange, electrodialysis, electrolysis [4]. Among these, adsorption of pollutants by means of porous materials has been regarded as the best choice because of its effectiveness, easy operation and low costs. Numerous applications have been reported in the literature concerning the development of inorganic sorbents such as clay minerals, zeolites and siliceous material [5,6], but carbon-based microporous organic polymers (MOPs) characterized by high specific surface area have recently emerged as outstanding materials for their performances in water remediation processes [7-9].

Widely applied in several fields for gas adsorption and separation [10,11], energy storage [12], molecular separation [13] drug delivery [14,15] and catalysis [16], MOPs have been used in water remediation processes to remove both cationic and anionic organic dyes, halogenated (i.e., trichloroethylene) and non-halogenated (i.e., polycyclic aromatic hydrocarbons) pollutants, pharmaceuticals and toxic metals [17-20].

MOPs typically used for water purification are covalent organic frameworks [21-23], hyper-crosslinked resins [24,25] and molecularly imprinted polymers [26,27]. Besides their high surface area, the great advantage of these sorbents relies on the possibility of chemically functionalize the surface of the material to selectively target specific pollutants [28-30]. MOPs have also been used to enhance the performances of conventional membrane devices, boosting their adsorbing properties and the working robustness [31,32].

In the last few years, to meet with the need for low cost, green and reusable materials, the potential of bio-inspired and/or biocompatible sorbents has also been explored [33-35]. Efficient results have been obtained by using natural polymers such as polysaccharides (i.e., cellulose and chitosan) [36-

41], gums, polyphenols (i.e., tannins, lignins) [42] and organic waste materials [43,44], proving efficient sorbents for the removal of dyes, pesticides, heavy metal cations and other pollutants. In line with this evidence, fungal melanins [45], the dark brown pigments biosynthesized by Ascomycetes starting from the metabolite 1,8-dihydroxynaphthalene (1,8-DHN), have emerged as valuable biosorbent for their ability to sequestrate/bioaccumulate toxic metals and drugs [46e51]. Recently, to face the low availability of these natural pigments on large scale, synthetic procedures have been developed allowing for the preparation in high yields of fungi-inspired melanin nanoparticles (pDHN-NPs) and based on the in vitro oxidative polymerization of the metabolic precursor, 1,8- DHN. The versatility of pDHN-NPs as functional material has been widely described in the literature. As generally reported for melanins, pDHN-NPs exhibit an intense absorption throughout the entire UVevisible spectrum and a good biocompatibility toward different cell lines and stem cells [52,53]. pDHN-NPs also proved to be effective radical quenchers not only by themselves (evidence from DPPH and FRAP antioxidant assays [54], but also when incubated in vitro in human cells by preventing the UV-induced accumulation of reactive oxygen species [55].

Recently, Gianneschi et al. reported on the high intrinsic microporosity (up to 860 m2/g) of a series of pDHN-NP analogues obtained via the oxidation of 1,8-DHN promoted by NaIO4 and their properties to capture gases (ammonia capture up to 17.0 mmol/g at 1 bar) and toxins (dimethyl methylphosphonate) when used as coating of fabrics with high breathability [56]. In line with these data, we report for the first time on the development of an innovative surface engineering process for the preparation of pDHN coated nylon membranes (pDHN-NMs) with high adsorbing properties toward the azo dye methylene blue (MB), responsible for the 17-20% of the industrial (textile, printing and cosmetic) contamination of water [57,58], able to cause psychosis, hypertension, nausea and, in the case of prolonged exposure, also carcinogenesis [59-63].

The data reported herein, compared with those collected for the bulk pDHN-NPs, highlight the enormous potential of this biosorbent and open up to new perspectives toward the design of a new generation of melanin-based filtering membranes for water remediation processes.

2. Materials and methods

2.1. Preparation of pDHN-NPs. The preparation of pDHN-NPs was carried out according to a procedure reported in the literature and based on the oxidative polymerization of 1,8-DHN under enzymatic conditions, namely horseradish peroxidase (HRP/H_2O_2), in phosphate buffer at pH 7.4 [64,65].

2.2. Preparation of pDHN-NMs. Commercially available nylon membranes (Chemtek analytica, pore size 0.45 μm, diameter 47 mm) were coated with pDHN melanin according to the ammonia-induced solid state polymerization protocol [66]. In brief, a methanol solution of 1,8-DHN (20mg/mL) was prepared and filtered before use. Aliquots of this solution (0.5 mL) were withdrawn and completely adsorbed onto a single nylon membrane. The nylon filter was dried under reduced pressure to remove the solvent and then exposed for 24 h to air-equilibrated ammonia vapours. Finally, the membrane was rinsed with water and washed three times and then dried under reduced pressure.

2.3. pDHN-NPs analysis. SEM analysis was performed on pDHN-NPs with a FEI Quanta 200 FEG SEM using a secondary electron detector and an acceleration voltage of 10–30 kV. Before analysis, small amounts of pDHN-NPs were deposited on aluminum stubs covered by carbon adhesive disks and the sample was sputter coated with gold/palladium.

TEM analysis was performed on pDHN-NPs before and after adsorption of MB: pDHN-NPs were dispersed in water and collected by dipping a carbon coated copper grid in the suspension; about 3 mg of pDHN-NPs were introduced in a vial containing 3 mL of a 20 mg/mL aqueous MB solution, then, after 24 h at 25 °C, pDHN-NPs were collected by dipping a carbon coated copper grid in the suspension. TEM analysis was performed in bright field mode using a FEI-Tecnai G12 Spirit Twin (LaB_6 source) operating at120 kV. TEM images were collected on a FEI Eagle 4k CCD camera.

Zeta-potential measurements were performed on pDHN-NPs at different pH values by laser Doppler micro-electrophoresis, using a Zetasizer Nano ZS (Malvern Instruments). pDHN-NPs were dispersed

at the concentration of 1 mg/mL in distilled water (pH 7), in a HCl solution at pH 3 and in a NaOH solution at pH 11 by sonication in a Transsonic Digitals ultrasonic bath for 5 min. Measurements were performed in triplicate at 25 °C.

2.4. pDHN-NMs analysis.

ATR-FTIR spectra in transmission mode have been recorded with a Nicolet 5700 spectrometer. The spectra have been scanned on the wavenumber range of 400-4000 cm^{-1} with the resolution fixed to 4 cm^{-1}.

Morphological analysis of the pristine filter and the filter coated with pDHN was performed by scanning electronic microscopy (SEM), using a FEI Quanta 200 FEG SEM (FEI, Eindhoven, The Netherlands), at 10 kV acceleration voltage, with a secondary electron detector. Before SEM observations, the samples were mounted on aluminum stubs and sputter coated with a 15 nm thick gold/palladium layer.

Tensile properties of the pristine filter and the filter coated with pDHN were analysed by means of a Deben microtensile test apparatus. Stress–strain curves were recorded with a 200 N load cell, setting the crosshead speed at 1 mm/min. Three specimens (5 mm wide, 0.165 mm thick, 10 mm gauge length) were analyzed for each sample and average Young's modulus, maximum tensile stress and elongation at break values were calculated.

2.5. Gas adsorption analysis. Gas adsorption volumetric analysis was performed on pDHN-NPs using a Micromeritics ASAP 2020 analyzer. The pDHN-NPs nitrogen adsorption/desorption isotherm at -196 °C was registered and their specific surface area was determined by using Brunauer-Emmett-Teller (BET) and Langmuir models. Nonlocal density functional theory (NLDFT) was applied to the nitrogen adsorption isotherms to evaluate the pore size distribution of the materials by using a carbon slit geometry and a N_2 DFT model. CO_2 adsorption/desorption measurements were also performed on pDHN-NPs with the same equipment at 0 °C and 25 °C, using a Micromeritics Iso Controller for the temperature control. pDHN-NPs were degassed at 100 °C under vacuum ($P < 10^{-5}$ mbar) before analyses and all adsorption measurements were performed using high purity gases (>99.999%). The

pDHN-NPs isosteric heats of CO_2 adsorption (Q_{st}) was calculated using the Clausius−Clapeyron equation from CO_2 adsorption isotherms.

2.6. MB adsorption tests in batch. MB solutions at a concentration of 5, 10, 20, 30, 50, 100, 250, 400 and 500 mg/L were prepared in deionized water. For the adsorption tests, in each experiment pDHN-NPs (10 mg) or pDHN-NMs were suspended in 10 mL of the dye solution and stirred at a rate of 250 rpm at ambient conditions (pH 6.5, 25 °C) until the equilibrium was reached (30 minutes). The MB concentration in the solution was measured at different interval times by using a Jasco V-560 UV-vis spectrophotometer (MB absorption maximum at λ_{max} = 663 nm).

In the case of pDHN-NPs, additional tests were carried out by changing the pH of the incubation mixtures. To this aim the initial pH of the solution was adjusted by adding dropwise 0.1 M NaOH or 0.1 M HCl solutions.

The adsorption capacity at equilibrium (Q_e) and the MB removal percentage (R) were calculated as follows:

$$Q_e = [(C_0\text{-}C_e)/W] \times V \quad (\mathbf{1})$$

$$R = [(C_0\text{-}C_e)/C_0] \times 100 \quad (\mathbf{2})$$

where C_0 and C_e are the initial and equilibrium dye concentration (mg/L), respectively; W (g) is the amount of used adsorbent; V (L) is the employed dye solution volume.

In all experiments the ratio between the volume of the dye solution and the adsorbent mass was kept equal to one.

2.7. In-flow MB adsorption tests. MB solutions at a concentration of 5, 10, 20, 30 mg/L were prepared in deionized water. For the adsorption tests, in each experiment a pDHN-NM was placed in a benchtop filtration device and used under a 0.1 bar pressure to purify 10 mL of the dye solution.

The MB concentration in the filtered solution was measured by using a Jasco V-560 UV-vis spectrophotometer (MB absorption maximum at λ_{max} = 663 nm).

2.8. Adsorption kinetics. The adsorption kinetics experiments were carried out by incubating pDHN-NPs (1 mg/mL) or pDHN-NMs into MB water solutions (pH 6.5, 25 °C) at different concentrations

of the dye (in the range 5-30 mg/L) and under stirring (rate = 250 rpm). The acquired data were fitted to the following Lagergren's pseudo first order (Equations **3** and **4**) and Ho's pseudo second order (Equations **5** and **6**) models:

$$dQ_t/dt = k_1(Q_e - Q_t) \quad (\mathbf{3})$$

$$\ln(Q_e - Q_t) = \ln Q_e - k_1 t \quad (\mathbf{4})$$

where Q_e and Q_t represent the quantity (mg/g) of dye adsorbed at equilibrium and at different interval times t and k_1 is the pseudo first order rate constant of adsorption (min^{-1}).

$$dQ_t/dt = k_2(Q_e - Q_t)^2 \quad (\mathbf{5})$$

$$t/Q_t = (1/k_2 Q_e^2) + t/Q_e \quad (\mathbf{6})$$

where k_2 is the pseudo second order rate constant of adsorption (g/(mg × min)).

2.9. Adsorption isotherm. The adsorption isotherms experiments were carried out by incubating pDHN-NPs (1 mg/mL) or pDHN-NMs into MB water solutions (pH 6.5, 25 °C) at different concentrations of the dye (in the range 5-500 mg/L) and under stirring (rate = 250 rpm). The data were adjusted to the following Langmuir (Equation **7**), Freundlich (Equation **8**) and Temkin (Equation **9**) isotherm models to investigate the mechanism of MB adsorption by pDHN-NPs:

$$C_e/Q_e = 1/Q_{max}K_L + C_e/Q_{max} \quad (\mathbf{7})$$

$$\ln Q_e = \ln K_F + 1/n \ln Ce \quad (\mathbf{8})$$

$$Q_e = B_T \ln A_T + B_T \ln C_e \quad (\mathbf{9})$$

where C_e is the equilibrium concentration (mg/L), Q_e is the amount of adsorbed dye at equilibrium (mg/g), Q_{max} (mg/g) is the theoretical maximum adsorption capacity; K_L (L/mg) is the Langmuir constant and K_F (mg/g) is the Freundlich constant, both related to the adsorption capacity, n is a constant related to the adsorption intensity. A_T is the Temkin binding energy constant at equilibrium (L/g), $B_T = RT/b$ is an indicator of the adsorption heat (J/mol), with T = absolute temperature (K), R = universal gas constant, b = Temkin isotherm constant.

2.10. Thermodynamic analysis. Thermodynamic analysis was performed by incubating pDHN-NPs (1 mg/mL) or pDHN-NMs into a 20 mg/L MB water solution (pH 6.5) at different temperatures (in

the range 30-60 °C) and under stirring (rate = 250 rpm). After 30 minutes incubation time, aliquots of the mixture were taken, subjected to UV-vis spectroscopic analysis for the determination of *Qe* and the thermodynamic parameters calculated according to the following equations **10**-**12**:

$$K = Q_e/C_e \quad (\mathbf{10})$$

$$\ln K = \Delta S^0/R - \Delta H^0/RT \quad (\mathbf{11})$$

$$\Delta G^0 = \Delta H^0 - T\Delta S^0 = -RT\ln K \quad (\mathbf{12})$$

2.11. pDHN-NPs regeneration tests. For the regeneration tests, a same stock of pDHN-NPs was subjected to seven adsorbing/desorbing cycles. The adsorption tests were performed by incubating 1 mg/mL of pDHN-NPs into MB water solutions (pH 6.5, 25 °C) at different concentrations (in the range 5-30 mg/L) and under stirring (rate = 250 rpm). After 30 minutes, aliquots of the mixture were withdrawn and analyzed by UV-vis spectroscopy. After each adsorbing step, pDHN-NPs were collected by centrifugation (7000 rpm, 15 min), rinsed with ethanol (10 mL) and treated with NaCl in an ultrasound bath for 30 minutes; then the solid was recovered by centrifugation (7000 rpm, 15 min). The procedure was repeated for several times until the ethanol solution became colorless. The precipitate was washed with water to remove NaCl, lyophilized and then reused.

2.12. pDHN-NMs regeneration tests. For the regeneration tests, the same pDHN-NM was subjected to seven adsorbing/desorbing cycles. The adsorption tests were performed by dipping the pDHN-NM into MB water solutions (pH 6.5, 25 °C) at different concentrations (in the range 5-30 mg/L) and under stirring (rate = 250 rpm). After 30 minutes, aliquots of the mixture were withdrawn and analyzed by UV-vis spectroscopy. After each adsorbing step, the pDHN-NM was collected and rinsed with ethanol (10 mL) under stirring for 30 minutes; then, after removing the solution, the same quantity of ethanol was added. This procedure was repeated for several times until the ethanol solution became colorless. The pDHN-NM was recovered from the solution, washed with water, dried under reduced pressure and then reused.

3. Results and discussion

3.1. Microporous melanin nanoparticles (pDHN-NPs): synthesis and characterization. The pDHN-NPs were prepared according to a procedure reported in the literature and based on the oxidative polymerization of 1,8-DHN, a commercially available fungal metabolite [64,65]. The synthetic approach meets the requisites of the green process, being carried out in phosphate buffer at physiological pH, with the sole addition of the enzymatic system horseradish peroxidase (HRP)/hydrogen peroxide and with no need for any purification step (Fig. 1). The pDHN-NPs can be easily recovered in high yields by centrifugation and used as are without further functionalization or treatment.

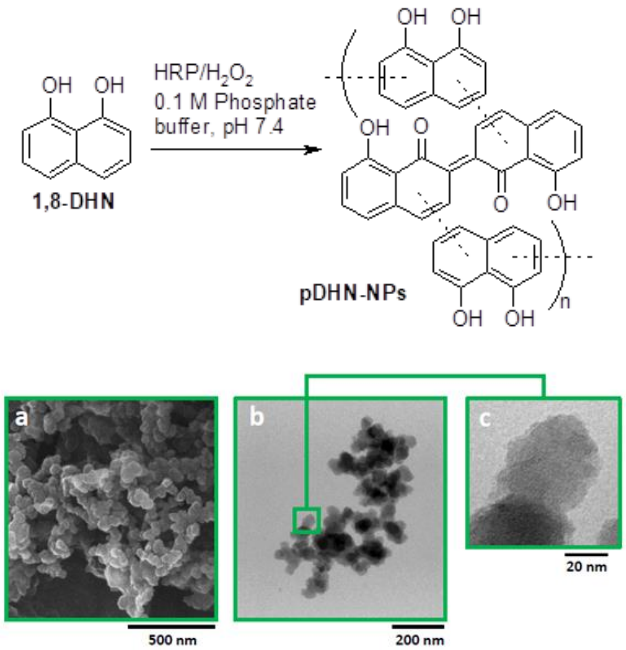

Fig. 1. Synthetic procedure for the preparation of pDHN-NPs (top) and SEM (a) and TEM (b, c) images of the nanoparticles (down).

In accord with literature data [52], the structural characterization of the pDHN-NPs, carried out by MALDI-MS analysis, ^{13}C cross-polarization/magic-angle-spinning (CP/MAS) NMR, UV-vis and ATR spectroscopies, supported the polymeric nature of the solid constituted by 1,8-dihydroxynaphthalene units, at different redox stages (phenol, extended quinone), linked via C-C

bonds (Fig. S1-S4). The morphological investigation carried out by SEM analysis (Fig. 1a) revealed the aggregate structure of pDHN-NPs, with the nanoparticle aggregates constituted by isodimensional primary particles. Moreover, TEM analysis (Fig. 1b,c) confirmed the quasi-spherical shape of the primary particles, whose average diameter is in the range 20-40 nm, connected in loose aggregates [52].

The pDHN-NP aqueous dispersions proved to be highly stable under a wide range of pH values, as denoted by the zeta potential measurements (Fig. S5) and in good agreement with previously reported data [56].

The adsorbing properties of pDHN-NPs were assessed by gas adsorption experiments (Fig. 2); in particular, nitrogen and carbon dioxide adsorption analyses were performed. The pDHN-NPs showed a type I nitrogen adsorption/desorption isotherm at -196 °C, which is typical of microporous materials, with a sharp saturation at high relative pressure, ascribable to nitrogen condensation in the nanoparticles interstitial voids (Fig. 2a). The pDHN-NPs were characterized by a Langmuir specific surface area (SSA) of 560 m^2/g and a total pore volume of 0.32 cm^3/g, 65 % of which is in the micropores range. Indeed, the nonlocal density functional theory (NLDFT) evidenced a prevalently microporous distribution, with a major peak centered at about 1.2 nm (Fig. 2b). Moreover, the pDHN-NPs showed carbon dioxide uptake capacity of 1.74 mmol/g and 2.24 mmol/g at 1 bar and 0 °C and 25 °C, respectively, (Fig. 2c) and heat of adsorption that varies from 35 to 20 kJ/mol in the 0.1 – 1.7 mmol/g range (Fig. 2d). These results indicate that the gas adsorption properties of pDHN-NPs are comparable to those of many high surface area MOPs, and are in good agreement with previously reported data on allomelanin nanoparticles [56].

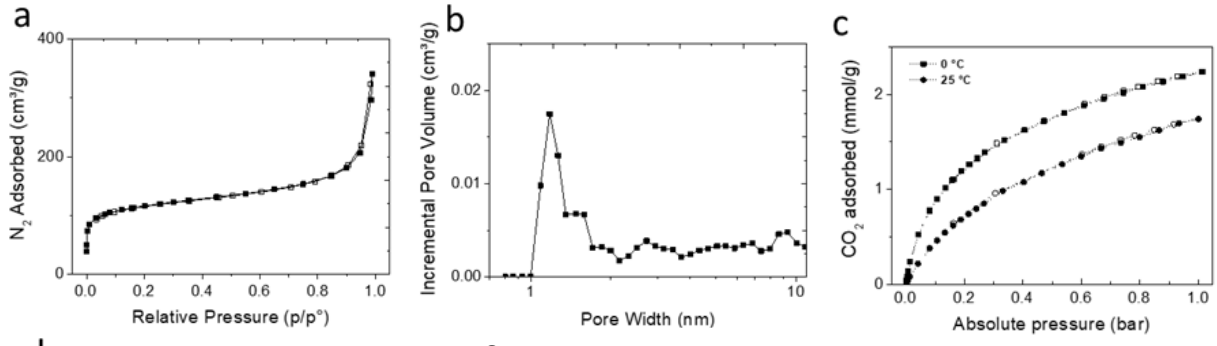

e

	pDHN-NPs
Langmuir SSA (m^2/g)	560 ± 8
BET SSA (m^2/g)	420 ± 4
Total pore volume (cm^3/g)[a]	0.32
Micropore fraction (%)	65
CO_2 uptake (mmol/g)[b]	2.24
CO_2 uptake (mmol/g)[c]	1.74

[a]Determined at $p/p^0 = 0.95$; [b]determined at 0 °C; [c]determined at 25 °C

Fig. 2. (a) pDHN-NPs nitrogen adsorption-desorption isotherm at -196 °C (adsorption in full points, desorption in hollow points); (b) NLDFT pore size distribution; (c) carbon dioxide adsorption-desorption isotherms at 0 °C and 25 °C (adsorption in full points, desorption in hollow points); (d) carbon dioxide heat of adsorption; (e) adsorption measurement data.

3.2. Preparation and characterization of pDHN coated nylon membranes (pDHN-NMs)

Commercially available nylon membranes (pore size 0.45 mm, diameter 47 mm) were coated with pDHN allomelanin by pursuing the ammonia induced solid state polymerization (AISSP) approach [66]. In brief, the nylon membrane was dipped into a methanolic solution of 1,8-DHN (20 mg/mL). After few minutes, when the complete adsorption of the 1,8-DHN solution onto the membrane was reached, the nylon filter was dried under reduced pressure to remove the solvent and then exposed for 24 h to air-equilibrated ammonia vapours. Finally, the membrane was rinsed with water and washed three times and then dried under reduced pressure to remove the traces of water.

Evidence for the successful coating came from the chromatic changes of the nylon filter passing from the white colouration of the pristine membrane to a pale-yellow colouration after 1,8-DHN coating and finally to a dark brown colouration typical of pDHN allomelanins (Fig. 3a).

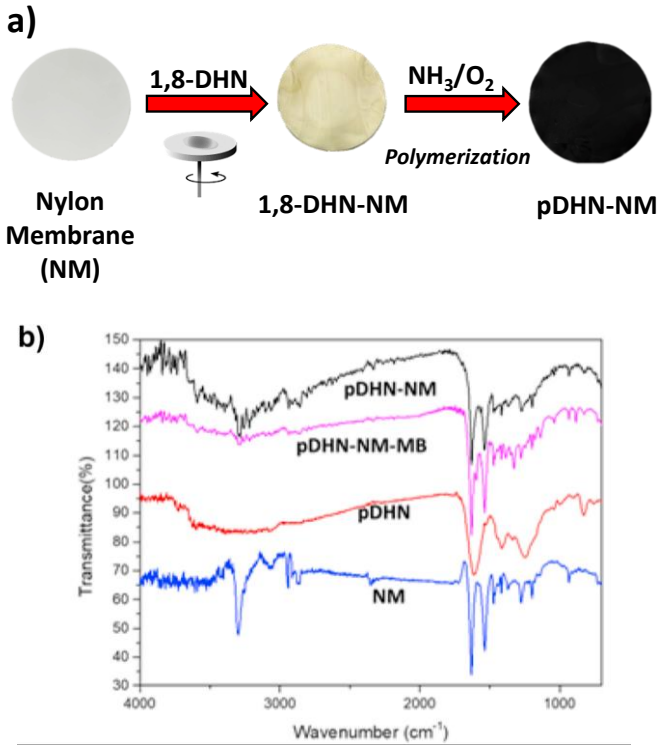

Fig. 3. Preparation of pDHN-NMs by AISSP technique (a); ATR-FTIR spectra of pristine nylon membrane (NM), pDHN, pDHN-NM and pDHN-NM after MB adsorption (pDHNNM-MB) (b).

The deposition of the pDHN coating was further supported by ATR spectroscopy. As shown in Fig. 3b, in the spectrum of the pDHN melanin coated nylon membrane (pDHN-NM) the stretching bands of the NM at 1,633 and 1,533 cm 1 and a broad band in the 3,000-3,600 cm^{-1} region ascribable to the O-H stretching characteristic of pDHN were clearly evident; also the bending band of the aromatic double bonds of pDHN at 1,622 cm^{-1}, the C-O stretching band of phenols at 1,410 cm^{-1} and the OeH bending band at 1,244 cm^{-1} were detected even if partially overlapped.

Morphological changes occurring on the membrane after the application of pDHN coatings were investigated by SEM analysis. The pristine membrane (Fig. 4a,b) showed the typical porous microfibrillar morphology of filter membranes prepared by phase inversion process, with pore size in the range of 1 µm. After the application of the pDHN coating (Fig. 4c), the porous structure and the pore size distribution is not significantly altered, thus indicating that the coating would not significantly affect the flow rate of the filter. On the other hand, the presence of the coating is clearly

evidenced at high magnification (Fig. 4d), with the presence of the typical particle morphology of pDHN, well anchored to the filter surface, without no indication of debonding phenomena.

Moreover, the coating application induced a slight but appreciable improvement of the tensile properties of the membranes. Stress strain curves of the pristine and pDHN-coated nylon disks are shown in Fig. 4e. In detail, the Young's modulus increased from 164 ± 5 Pa for the pristine filter to 186 ± 3 Pa, whereas the maximum tensile stress increased from 5.2 ± 0.2 Pa to 5.7 ± 0.2 Pa. Furthermore, as a consequence of the coating application, only a slight decrease of the elongation at break was recorded, from 7.8 % to 7.2 %, this difference being lower than standard deviation values on the measures (± 1.1 % for both samples).

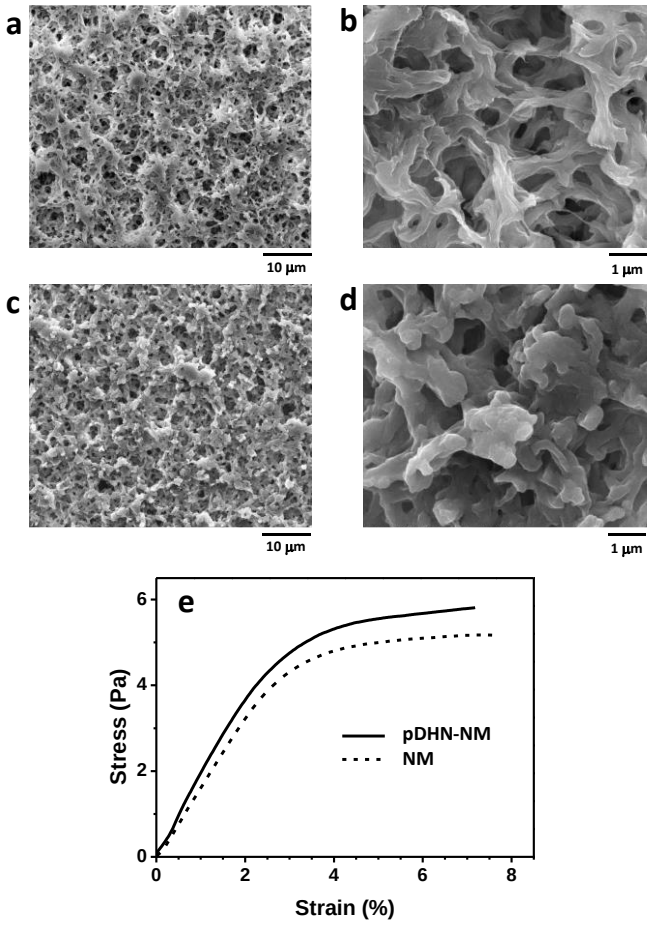

Fig. 4. SEM images of the pristine nylon membrane (a, b) and of the pDHN-NM (c,d); stress strain analysis of the filtering membranes.

3.3. Methylene blue adsorption tests. The ability of pDHN to remove MB from water was tested both in the case of pDHN-NPs and in the case of pDHN-NMs. Preliminary experiments were carried out in batch by incubating the melanin nanoparticles (1 mg/mL) or the melanin-coated membrane (0.6 mg/cm^2) into a 20 mg/L water solution of the dye.

As shown in Fig. 5a,b, in both cases the typical blue colouration of the dye completely disappeared in the water solution after 30 minutes incubation time, suggesting that the adsorption of MB had occurred. This evidence was also supported by the investigation of the UV-visible spectrophotometric course of the water treatment. The spectra reported in Fig. S6 showed that the absorption maxima of the dye at 613 and 663 nm rapidly slowed down after the addition of pDHN-NPs, with 80% of MB removal registered after 5 minutes, indicative of a very fast process (Fig. 5c). The adsorption process proved to be slower in the case of pDHN-NMs with 65% of MB removal measured after the same time, as a result of the different permeability of the pDHN-coated membrane with respect to the melanin nanoparticles (Fig. 5d-f).

After MB adsorption, no significant morphological changes of the coating were evident (Fig. S8), confirming the good adhesion and stability of the pDHN melanin layer on the membrane.

To check if the disappearance of the blue colour was due to the dye adsorption by pDHN rather than to the reduction of the dye promoted by the melanin polymer, the water incubation mixture was recovered and subjected to ^{1}H NMR spectroscopy. This revealed the complete absence of signals ascribable to protons of the reduced form of MB, so indicating that the dye was completely adsorbed by the allomelanin polymer. The adsorption was also supported by TEM images of pDHN-NPs collected after the incubation with the water solution of MB (Fig. S7), showing a reduced contrast of the NPs due to the surface adsorption of the organic dye, in comparison to TEM images of pristine NPs (Fig. 1).

Moreover, the FT-IR spectrum of the pDHN-NM after the absorption of the dye showed the appearance of three bands assigned to MB at 1,328 cm^{-1}, due to C-N stretching, and at 1,598 and 1,386 cm^{-1}, due to vibrations of the aromatic double bonds (Fig. 3).

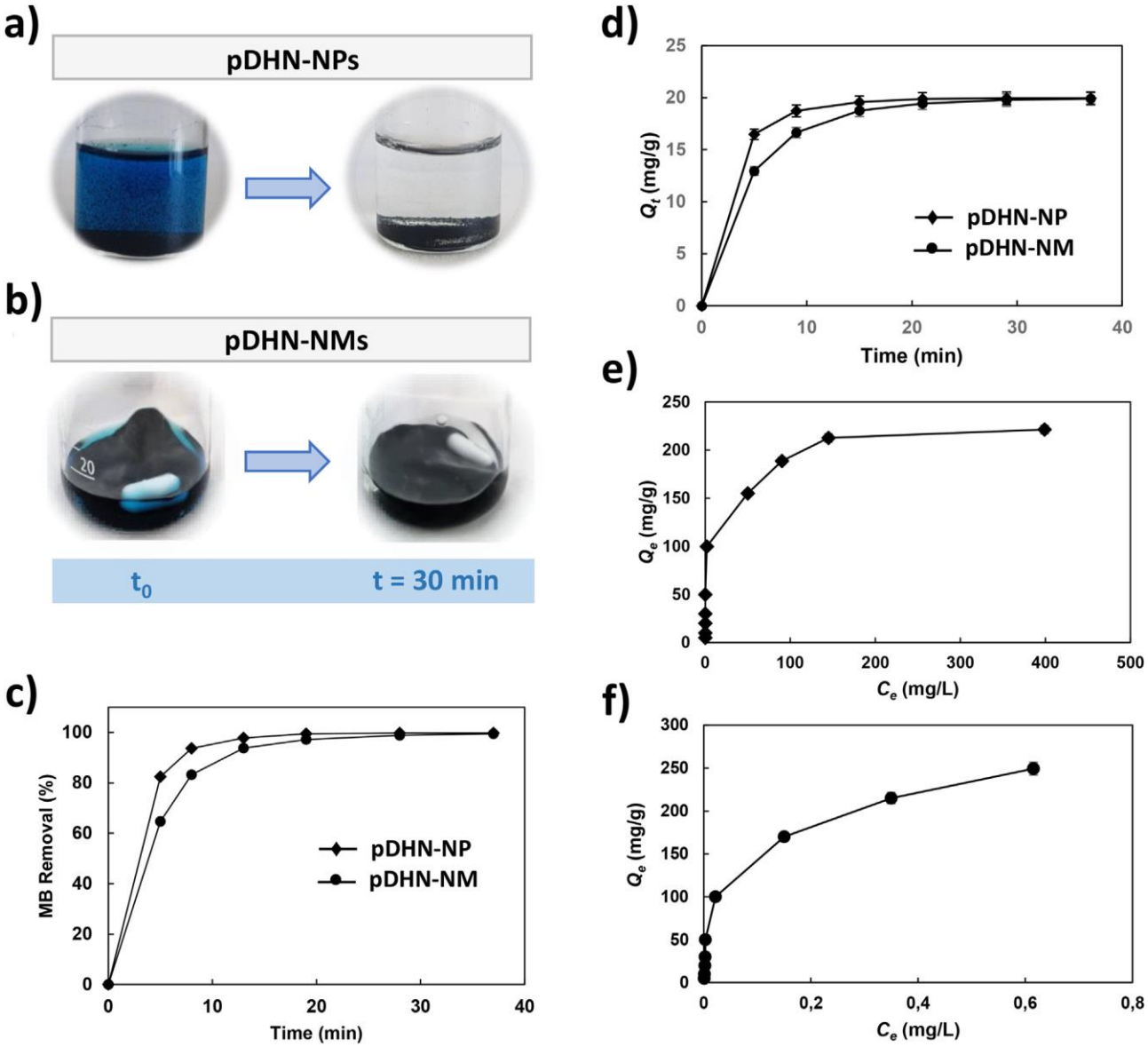

Fig. 5. MB removal by pDHN-NPs. Incubation mixture: 20 mg/L water solution of MB, 1 mg/mL pDHN-NPs (a); MB removal by pDHN-NMs. Incubation mixture: 20 mg/L water solution of MB (b); time course of the MB removal (c) and Qt values (d) by treatment with pDHN-NPs and pDHN-NMs; correlation between the adsorption capacity at equilibrium (Qe) and the equilibrium dye concentration (Ce) for pDHN-NPs (e) and pDHN-NMs (f). The reported results represent the mean ± SD of three separate experiments.

Equilibrium adsorption tests performed at different dye concentrations (in the range 5-500 mg/L) revealed that, in the case of pDHN-NPs, the MB uptake at equilibrium (Q_e) increased from 5.0 to 221.3 mg/g as the initial MB concentration increased from 5 to 500 mg/L, suggesting a significant dependency of the dye adsorption with its initial concentration (Table S1). Accordingly, the MB removal proved to be quite high (> 99%) for MB concentrations in the range 5-100 mg/L, whereas a marked reduction was observed for higher concentrations (500 mg/L). This effect can be considered as a consequence of the steric hindrance occurring on the surface of the pDHN-NPs with the saturation of the adsorption sites.

A similar trend was observed also in the case of pDHN-NMs, but a higher efficiency in the adsorption properties was clearly evident, despite the constant contribution of the pristine membrane, with a MB removal > 99% for dye concentrations up to 250 mg/L (Table S2).

In the case of pDHN-NPs, the high MB removal efficiency proved not to be affected by the pH (Fig. 6a) or the ionic strength (Fig. 6b) of the water solution, with over the 99% of MB being adsorbed independently from the initial concentration of the dye. These data suggest that the interaction between MB and pDHN: a) could not suffer the high concentration of the salts typically found in industrial wastewater; b) is mainly driven by hydrogen bonding, π–π and n-π interactions, and micropore filling (Fig. 6c) [67]. The electrostatic interactions proved not to be so efficient considering that the MB removal was as high as 99% even below pH 6, when the phenolic groups on pDHN are not dissociated.

To check for the efficiency of pDHN-NMs in removing MB from water by filtration under reduced pressure, the melanin-coated filter was placed in a benchtop filtration device and used under a 0.1 bar pressure. As anticipated by the analysis of the SEM images, the flow rate of water filtration proved not to be affected by the melanin coating. Different MB solutions, with concentrations ranging from 5 to 30 mg/L, were filtered by using the pristine nylon membranes or the corresponding melanin-coated membranes. As shown in Fig. 7, pDHN-NMs proved to be more efficient in the dye removal, with <1% of MB released into the filtered water. The pristine membranes were also able to

partially adsorb MB but in lower amounts, confirming the active role played by the melanin coating in enhancing the adsorbing properties of the membrane.

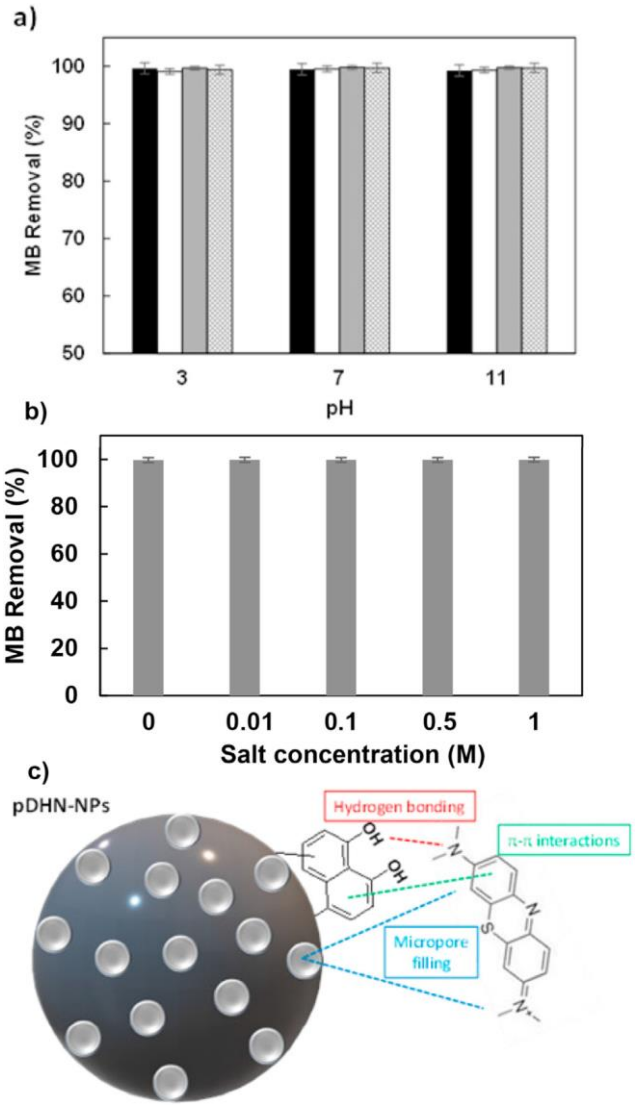

Fig. 6. (a) MB removal by pDHN-NPs at different pH values. MB concentration: 5 mg/L (black bars), 10 mg/L (white bars), 20 mg/L (grey bars) and 30 mg/L (dotted bars). (b) MB removal by pDHN-NPs at different ionic strength values. MB concentration: 20 mg/L, pH: 7, t = 30 min. The reported results represent the mean ± SD of three separate experiments. c) Proposed mechanism of adsorption of MB on pDHN-NPs.

.

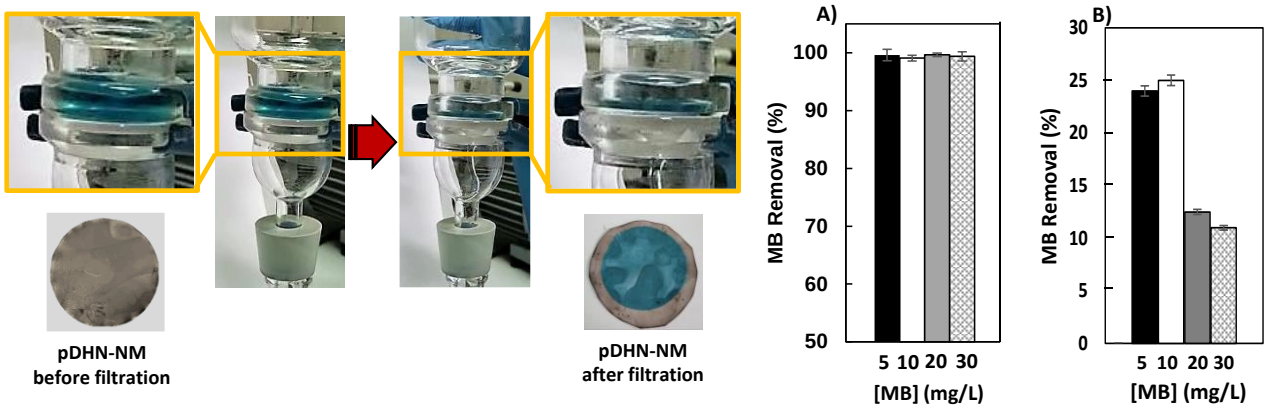

Fig. 7. In-flow MB removal by pDHN-NMs. Pictures of the filtering device and of the pDHN-NM before and after MB adsorption (left panel); MB removal efficiency of the pDHN-NM (A) and of the pristine NM (B) with different MB concentrations (right panel). The reported results represent the mean ± SD of three separate experiments.

3.4. Adsorption isotherms. To further delineate the interaction mechanism between MB and pDHN, the experimental data of the adsorption process were fitted with the isotherm models of Langmuir, Freundlich and Temkin. The Langmuir model describes the monolayer adsorption process on a surface with homogeneous sites, whereas the Freundlich model imply a multilayer adsorption process on a heterogenous surface; the Temkin model contains a factor that explicitly takes into account the heat of adsorption.

The Langmuir, Freundlich and Temkin isotherm models are described by the following equations **7-9**:

$$C_e/Q_e = 1/Q_{max}K_L + C_e/Q_{max} \quad \textbf{(7a)}$$

$$\ln Q_e = \ln K_F + 1/n \ln Ce \quad \textbf{(8a)}$$

$$Q_e = B_T \ln A_T + B_T \ln C_e \quad \textbf{(9a)}$$

where C_e is the equilibrium concentration (mg/L), Q_e is the amount of adsorbed dye at equilibrium (mg/g), Q_{max} (mg/g) is the theoretical maximum adsorption capacity, K_L (L/mg) is the Langmuir constant, K_F (mg/g) is the Freundlich constant, both related to the adsorption capacity, n is a constant

related to the adsorption intensity. Values of n within the range 1 - 10 are indicative of an efficient adsorption process. A_T is the Temkin binding energy constant at equilibrium (L/g), B_T = RT/b is an indicator of the adsorption heat (J/mol), with T = absolute temperature (K), R = universal gas constant, b = Temkin isotherm constant.

Table 1. Isotherm parameters calculated according to the Langmuir, Freundlich and Temkin models for pDHN-NPs and pDHN-NMs.

	pDHN-NPs	**pDHN-NMs**
Langmuir adsorption model		
Q_{max} (mg/g)	220.5	262.2
K_L (L/mg)	0.4	31.5
r^2	0.998	0.997
Freundlich adsorption model		
n	3.3	1.9
K_F (mg/g)	50.1	481
r^2	0.740	0.658
Temkin adsorption model		
B_T (J/mol)	22.2	38.7
A_T (L/mg)	73.0	866.4
r^2	0.963	0.991

The Langmuir, Freundlich and Temkin parameters are reported in Table 1, whereas the corresponding plots are reported in Fig. S9-S10. In both cases, the results highlighted the best fit of the Langmuir isotherm model with the experimental data, with a correlation coefficient r^2 of 0.998 for pDHN-NPs and 0.997 for pDHN-NMs, indicating that a monolayer adsorption occurred on the homogeneous surface of pDHN. The good correlation coefficient observed also for the fitting with the Temkin isotherm model (r^2 = 0.963 and 0.991) suggests that the MB adsorption process is exothermic and driven by physisorption, as denoted by the B_T value.

To further evaluate the feasibility of the MB adsorption process, the separation factor R_L related to the Langmuir isotherm model was calculated as follows:

$$R_L = 1/(1 + K_L C_0) \quad (\mathbf{13})$$

The R_L value is indicative of irreversible ($R_L = 0$), favourable ($0 < R_L < 1$), linear ($R_L = 1$) and unfavourable ($R_L > 1$) adsorption processes. The R_L values calculated for the MB adsorption were in the range 0.005 – 0.3, for pDHN-NPs, and in the range $0.006 – 6 \times 10^{-5}$, for pDHN-NMs, suggesting in both cases favourable process. According to the Langmuir model the maximum adsorption capacities of MB onto pDHN-NPs and pDHN-NMs are 220 and 262 mg/g, respectively. These represent quite high values for a biosorbent if we consider that no treatment has been carried out to improve its adsorbing properties, comparable to those obtained from inorganic porous materials (Table S3) [68].

3.4. Kinetic analysis. The kinetic analysis has been performed to delineate more accurately the reaction rate between the adsorbent, pDHN, and the adsorbate, MB. Two kinetic equation models, Lagergren's pseudo first order and the Ho's pseudo second order models, have been adopted to evaluate the adsorption kinetics of MB onto pDHN-NPs. Both models have been used for adsorption processes carried out at 25 °C and at a pH value of 6.5 varying the MB concentration.

Lagergren's model is described by the following equations **3** and **4**:

$$dQ_t/dt = k_1(Q_e - Q_t) \quad (\mathbf{3a})$$

$$\ln(Q_e - Q_t) = \ln Q_e - k_1 t \quad (\mathbf{4a})$$

where Q_e and Q_t represent the quantity (mg/g) of dye adsorbed at equilibrium and at different interval times t and k_1 is the pseudo first order rate constant of adsorption (min^{-1}).

Ho's model is described by the following equations **5** and **6**:

$$dQ_t/dt = k_2(Q_e - Q_t)^2 \quad (\mathbf{5a})$$

$$t/Q_t = (1/k_2 Q_e^2) + t/Q_e \quad (\mathbf{6a})$$

where k_2 is the pseudo second order rate constant of adsorption (g/mg×min).

In Fig. 8 are reported the linear plots of $\ln(Q_e - Q_t)$ and $\frac{t}{Q_t}$ versus t, that were used to calculate Q_e (Q_e^{calc}), k_1 and k_2 values for incubation mixtures of pDHN-NPs and pDHN-NMs at different MB

initial concentrations, and the corresponding kinetic data along with the correlation coefficient (r^2) and the experimental Q_e (Q_e^{exp}) values are reported in Table 2.

Both the r^2 values and the accordance between the Q_e^{calc} and Q_e^{exp} values suggested that the MB adsorption process underwent a pseudo second order kinetics with a rate constant k_2 decreasing with the increase of the initial concentration of the dye.

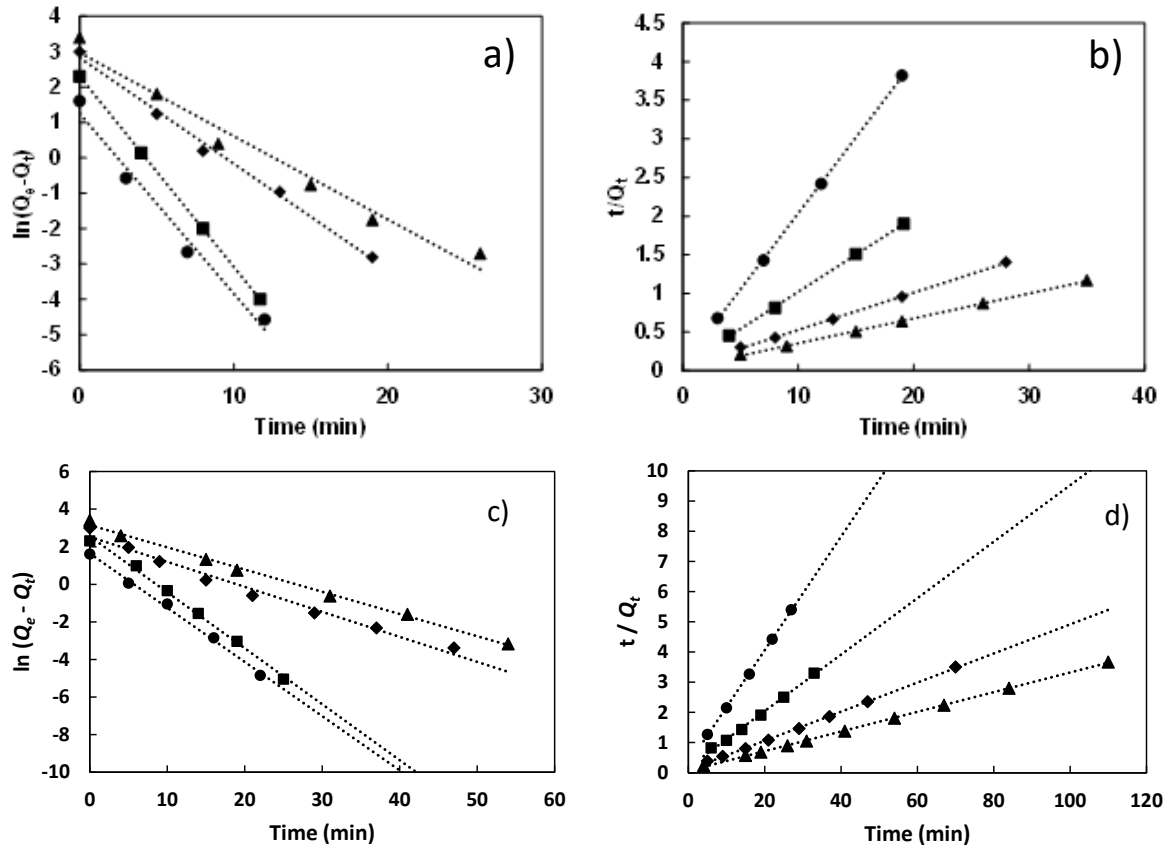

Fig. 8. Pseudo first order (a,c) and pseudo second order (b,d) plots for MB adsorption on pDHN-NPs (a,b) and pDHN-NMs (c,d). MB initial concentration: 5 mg/L (●), 10 mg/L (■), 20 mg/L (♦) and 30 mg/L (▲).

Table 2. Kinetic parameters obtained from application of pseudo first order and pseudo second order models to the adsorption of MB by pDHN-NPs and pDHN-NMs.

		Pseudo first order model			**Pseudo second order model**		
$[MB]_{ini}$ (mg/L)	**$Q_{e,}^{exp}$ (mg/g)**	**K_1 (min^{-1})**	**$Q_{e,}^{cal}$ (mg/g)**	**r^2**	**K_2 (g/mg×min)**	**$Q_{e,}^{cal}$ (mg/g)**	**r^2**

pDHN-NPs							
5	4.97	0.51	3.46	0.98	0.55	5.08	0.99
10	9.95	0.54	9.91	1.00	0.15	10.41	0.99
20	19.95	0.30	16.88	0.99	0.05	20.80	0.99
30	29.92	0.24	19.44	0.97	0.03	31.00	0.99
pDHN-NMs							
5	4.99	0.24	4.25	0.99	0.12	5.32	1.00
10	9.99	0.30	12.86	1.00	0.05	10.71	1.00
20	19.99	0.13	12.50	0.98	0.02	20.74	1.00
30	29.99	0.10	17.68	0.99	0.02	30.75	1.00

3.5. Thermodynamic analysis. Finally, the nature of the adsorption process of MB on pDHN-NPs and pDHN-NMs has been investigated from the thermodynamic point of view. To this aim, the Gibbs free energy change (ΔG°), the enthalpy change (ΔH°) and the entropy change (ΔS°) were calculated according to the following equations **10** and **11**:

$$K = Q_e/C_e \qquad (\mathbf{10a})$$

$$\ln K = \Delta S^0/R - \Delta H^0/RT \qquad (\mathbf{11a})$$

where K is the equilibrium constant of the adsorption process, R is the universal gas constant (8.314 J/mol×K) and *T* is the system temperature (K).

By plotting lnK as a function of 1/*T*, the ΔS° and ΔH° values were calculated (Table 3) as the intercept and slope of the linear regression (Fig. s S11 and S12), whereas the ΔG° value was calculated by applying the following equation **12**:

$$\Delta G^0 = \Delta H^0 - T\Delta S^0 = -RT\ln K \qquad (\mathbf{12a})$$

The negative ΔG° values clearly indicate that the adsorption process is spontaneous and favourable; moreover, the negative ΔH° value proved that the MB adsorption is an exothermic process, in good agreement with data obtained from equilibrium isotherms (Table 1).

Table 3. Thermodynamic parameters calculated for the adsorption of MB onto pDHN-NPs and pDHN-NMs determined at 20mg/L MB concentration and at pH 6.5.

T **(K)**	**ΔG (kJ·mol^{-1})**	**ΔH (kJ·mol^{-1})**	**ΔS (kJ·mol^{-1}·K^{-1})**
pDHN-NPs			
303	-19.49	-52.72	-0.11
313	-18.39		
323	-17.30		
333	-16.20		
pDHN-NMs			
303	-25.83	-124.92	-0.33
313	-22.54		
323	-19.23		
333	-15.92		

3.7. Recycling properties. To complete the overview on the performance of pDHN as new sustainable sorbent for MB, the reuse property both of the melanin nanoparticles and of the melanin-coated membranes were evaluated. This latter is a fundamental requisite because contributes to significantly abate the costs of the remediation process. To this aim, the same stock of pDHN-NPs or the same melanin-coated membrane was subjected to repeated adsorbing/desorbing cycles; these latter were performed by treating the pDHN-NPs or pDHN-NMs with a solution of NaCl in ethanol. In Fig. 9 are reported the MB removal efficiencies obtained starting from different MB concentration (from 5 to 30 mg/L) measured up to 7 adsorbing/desorbing cycles. As shown, the performance of the sorbing material is quite high for all the seven cycles with the MB removal efficiency that never goes under the 90% value, independently from the initial dye concentration. In particular, a straightforward result was obtained in the case of pDHN-NMs for which the MB removal efficiency proved not to be affected during the 7 adsorbing/desorbing cycles, suggesting the higher performance with respect to

pDHN-NPs. Overall, these data indicate that both pDHN-NPs and pDHN-NMs can be reused preserving almost the same dye removal efficiency, opening to many possibilities for their practical application in water remediation processes ensuring low environmental impact and industrial costs.

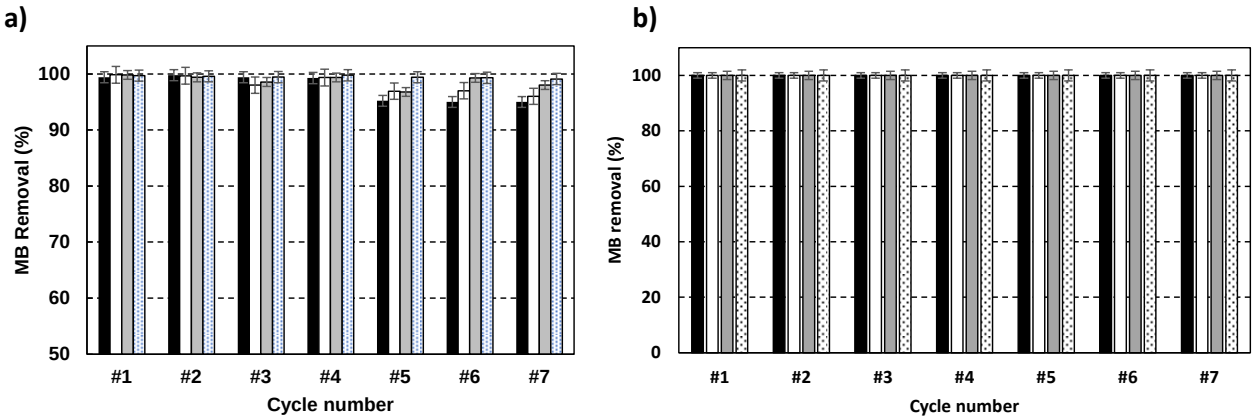

Fig. 9. Recycling performance for MB removal by pDHN-NPs (a) and pDHN-NMs (b). MB initial concentration: 5 mg/L (black bar), 10 mg/L (white bar), 20 mg/L (grey bar) and 30 mg/L (dotted bar). The results represent the mean $\pm$ SD of three separate experiments.

4. Conclusions

The continuous search for bio-inspired adsorbing materials is of utmost importance for their environmentally friendly profile improving the sustainability of our lifestyle. In this regard, pDHN represents a valid example of such materials for the following reasons: a) it has been designed taking inspiration from the fungal allomelanin polymers and in a recent paper its biocompatibility has been widely demonstrated; b) pDHN is a low-cost material, easily accessible via a one-step oxidation protocol and useable as is without any further purification/functionalization; c) pDHN is a versatile biomaterial that can be easily processed as functional coating on different kind of substrates. In this paper, we have demonstrated for the first time the ability of pDHN to efficiently sequestrate the MB dye both in batch experiments, when used as bulk nanoparticles, and in in-flow experiments, when used as coating of nylon membranes. This latter case proved to be particularly interesting because: a)

the porous structure of the nylon membrane was retained after the pDHN coating; b) the adsorption performance of the pDHN-NM proved to be quite high (maximum absorption capacity of 262 mg/g) even during the in-flow processes when the contact time between the water solution and the biosorbent is very short; c) the pDHN-NM proved to be reusable up to seven cycles without affecting the MB absorbing properties; d) the pDHN coating on the nylon membrane proved to be highly stable and resistant even after its reuse.

Thanks to the pDHN microporous morphology and to the peculiar surface chemical multifunctionality, the adsorbing process is fast, spontaneous and thermodynamically favoured, governed by physisorption, following a pseudo-first order kinetic and fitting quite well the Langmuir isotherm model, indicative of a monolayer adsorption on homogeneous sites.

Overall, these data open new perspectives toward the application of pDHN for the design of sustainable filtering devices for water/wastewater treatments.

Author contributions. Valeria Lino and Rachele Castaldo contributed equally to the design, execution and elaboration of the of the scientific experiments. Paola Manini and Gennaro Gentile contributed to the conceptualization of the paper, general supervision of the experimental work and data analysis, writing of the paper.

Declaration of competing interest. The authors declare that they have no competing interests.

Acknowledgements. This study has been carried out in the frame of the project SAPIENT (2017CBHCWF) funded by MIUR (PRIN – 2017) (PM and VL).

References and note

[†]VL and RC contributed equally to the design, execution and elaboration of the of the scientific experiments.

[1] A.S. Adeleye, J.R. Conway, K. Garner, Y. Huang, Y. Su, A.A. Keller, Engineered nanomaterials for water treatment and remediation: Costs, benefits, and applicability, Chem. Engin. J. 286 (2016) 640–662. https://doi.org/10.1016/j.cej.2015.10.105.

[2] F. Lu, D. Astruc, Nanocatalysts and other nanomaterials for water remediation from organic pollutants, Coord. Chem. Rev. 408 (2020) 213180. https://doi.org/10.1016/j.ccr.2020.213180

[3] C. Santhosh, V. Velmurugan, G. Jacob, S. K. Jeong, A. N. Grace, A. Bhatnagar, Role of nanomaterials in water treatment applications: A review, Chem. Eng. J. 306 (2016) 1116–1137. https://doi.org/10.1016/j.cej.2016.08.053

[4] A. Nagar, T. Pradeep, Clean Water through Nanotechnology: Needs, Gaps, and Fulfillment, ACS Nano 14 (2020) 6420–6435. https://doi.org/10.1021/acsnano.9b01730

[5] S.S. Gupta, K.G. Bhattacharyya, Adsorption of heavy metals on kaolinite and montmorillonite: a review, Phys. Chem. Chem. Phys. 14 (2012) 6698–6723. https://doi.org/10.1039/C2CP40093F

[6] S. Wang, Y. Peng, Natural zeolites as effective adsorbents in water and wastewater treatment, Chem. Eng. J. 156 (2010) 11–24. https://doi.org/10.1016/j.cej.2009.10.029

[7] V. Gupta, T. Saleh, Sorption of pollutants by porous carbon, carbon nanotubes and fullerene – an overview, Environ. Sci. Pollut. Res. 20 (2013) 2828–2843. https://doi.org/10.1007/s11356-013-1524-1.

[8] Z. Niu, L. Liu, L. Zhang, X. Chen, Porous Graphene Materials for Water Remediation, Small 10 (2014) 3434–3441. https://doi.org/10.1002/smll.201400128

[9] Q. Sun, B. Aguila, T. Song, S. Ma, Tailored Porous Organic Polymers for Task-Specific Water Purification, Acc. Chem. Res. 53 (2020) 812−821. https://doi.org/10.1021/acs.accounts.0c00007

[10] P. Bernardo, E. Drioli, G. Golemme, Membrane gas separation: A review/state of the art, Ind. Eng. Chem. Res. 48 (2009) 4638–4663. https://doi.org/10.1021/ie8019032.

[11] R. Dawson, A.I. Cooper, D.J. Adams, Nanoporous organic polymer networks, Prog. Polym. Sci. 37 (2012) 530–563. https://doi.org/10.1016/j.progpolymsci.2011.09.002.

[12] J. Weickert, R.B. Dunbar, H.C. Hesse, W. Wiedemann, L. Schmidt-Mende, Nanostructured organic and hybrid solar cells, Adv. Mater. 23 (2011) 1810–1828. https://doi.org/10.1002/adma.201003991

[13] C. Lu, S. Liu, J. Xu, Y. Ding, G. Ouyang, Exploitation of a microporous organic polymer as a stationary phase for capillary gas chromatography, Anal. Chim. Acta 902 (2016) 205–211. https://doi.org/10.1016/j.aca.2015.10.034

[14] B. Li, X. Yang, L. Xia, M.I. Majeed, B. Tan, Hollow microporous organic capsules, Sci. Rep. 3 (2013) 2128. https://doi.org/10.1038/srep02128

[15] S. Merino, C. Martín, K. Kostarelos, M. Prato, E. Vázquez, Nanocomposite hydrogels: 3D polymer–nanoparticle synergies for on-demand drug delivery, ACS Nano 9 (2015) 4686–4697. https://doi.org/10.1021/acsnano.5b01433

[16] C. Perego, R. Millini, Porous materials in catalysis: Challenges for mesoporous materials, Chem. Soc. Rev. 42 (2013) 3956–3976. https://doi.org/10.1039/C2CS35244C

[17] F. Lu, D. Astruc, Nanomaterials for removal of toxic elements from water, Coord. Chem. Rev. 356 (2018) 147–164. https://doi.org/10.1016/j.ccr.2017.11.003

[18] S. Wang, H. Sun, H.M. Ang, M.O. Tadé, Adsorptive remediation of environmental pollutants using novel graphene-based nanomaterials, Chem. Eng. J. 226 (2013) 336–347. https://doi.org/10.1016/j.cej.2013.04.070

[19] J.G. Yu, X.H. Zhao, H. Yang, X.H. Chen, Q. Yang, L.Y. Yu, J.H. Jiang, X.Q., Chen, Aqueous adsorption and removal of organic contaminants by carbon nanotubes, Sci. Total Environ. 482–483 (2014) 241–251. https://doi.org/10.1016/j.scitotenv.2014.02.129

[20] F. Yu, Y. Li, S. Han, J. Ma, Adsorptive removal of antibiotics from aqueous solution using carbon materials, Chemosphere 153 (2016) 365–385. https://doi.org/10.1016/j.chemosphere.2016.03.083

[21] H. Fan, J. Gu, H. Meng, A. Knebel, J. Caro, High-flux membranes based on the covalent organic framework COF-LZU1 for selective dye separation by nanofiltration, Angew. Chem. Int. Ed. 57 (2018) 4083-4087. https://doi.org/10.1002/anie.201712816

[22] Y. Li, C.X. Yang, H.L. Qian, X. Zhao, X.P. Yan, Carboxyl-functionalized covalent organic frameworks for the adsorption and removal of triphenylmethane dyes, ACS Appl. Nanomater, (2019) 7290-7298. https://doi.org/10.1021/acsanm.9b01781

[23] Y. Pi, X. Li, Q. Xia, J. Wu, Y. Li, J. Xiao, Z. Li, Adsorptive and photocatalytic removal of Persistent Organic Pollutants (POPs) in water by metal-organic frameworks (MOFs), Chem. Eng. J. 337 (2018) 351–371. https://doi.org/10.1016/j.cej.2017.12.092

[24] R. Castaldo, R. Avolio, M. Cocca, G. Gentile, M.E. Errico, M.C. Avella, C. Carfagna, V. Ambrogi, A Versatile Synthetic Approach toward Hyper-Cross-Linked Styrene-Based Polymers and Nanocomposites, Macromolecules 50 (2017) 4132. https://doi.org/10.1021/acs.macromol.7b00812.

[25] R. Castaldo, G. Gentile, M. Avella, C. Carfagna, V. Ambrogi, Microporous hyper-crosslinked polystyrenes and nanocomposites with high adsorption properties: A review, Polymers 9 (2017) 651. https://doi.org/10.3390/polym9120651.

[26] M. Cantarella, S.C. Carroccio, S. Dattilo, R. Avolio, R. Castaldo, C. Puglisi, V. Privitera, Molecularly imprinted polymer for selective adsorption of diclofenac from contaminated water, Chem. Eng. J. 367 (2019) 180-188. https://doi.org/10.1016/j.cej.2019.02.146.

[27] D.L. Huang, R.Z. Wang, Y.G. Liu, G.M. Zeng, C. Lai, P. Xu, C. Huang, Application of molecularly imprinted polymers in wastewater treatment: a review, Environmental Science and Pollution Research 22 (2015) 963-977. https://doi.org/10.1007/s11356-014-3599-8

[28] R. Castaldo, V. Ambrogi, R. Avolio, M. Cocca, G. Gentile, M.E. Errico, M. Avella, Functional hyper-crosslinked resins with tailored adsorption properties for environmental applications, Chem. Eng. J 362 (2019) 497. https://doi.org/10.1016/j.cej.2019.01.054

[29] R. Castaldo, R. Avolio, M. Cocca, M.E. Errico, M. Avella, G. Gentile, Amino-functionalized hyper-crosslinked resins for enhanced adsorption of carbon dioxide and polar dyes, Chem. Eng. J. 418 (2021) 129463. https://doi.org/10.1016/j.cej.2021.129463

[30] X.Q. Cheng, Z.X. Wang, J. Guo, J. Ma, L. Shao, Designing Multifunctional Coatings for Cost-Effectively Sustainable Water Remediation, ACS Sustainable Chem. Eng. 6 (2018) 1881−1890. https://doi.org/10.1021/acssuschemeng.7b03296.

[31] M.M. Pendergast, E.M.V. Hoek, A Review of Water Treatment Membrane Nanotechnologies, Energy Environ. Sci. 4(6), (2011) 1946−1971. https://doi.org/10.1039/C0EE00541J

[32] H. Gholami Derami, Q. Jiang, D. Ghim, S. Cao, Y.J. Chandar, J.J. Morrissey, Y.-S. Jun, S.A. Singamaneni, Robust and Scalable Polydopamine/Bacterial Nanocellulose Hybrid Membrane for Efficient Wastewater Treatment. ACS Applied Nano Materials, 2 (2), (2019) 1092−1101. https://doi.org/10.1021/acsanm.9b00022

[33] G. Crini, Non-conventional low-cost adsorbents for dye removal: A review, Biores. Technol. 97 (2006) 1061–1085. https://doi.org/10.1016/j.biortech.2005.05.001.

[34] J.R. Dodson, H.L. Parker, A.M. Garcia, A. Hicken, K. Asemave, T.J. Farmer, H. He, J.H. Clark, A.J. Hunt, Bio-derived materials as a green route for precious & critical metal recovery and re-use, Green Chem. 17 (2015) 1951–1965. https://doi.org/10.1039/C4GC02483D

[35] H. Feng, Y.N. Liang, X. Hu, Natural organic matter (NOM), an underexplored resource for environmental conservation and remediation, Mater. Today Sustain. 19 (2022) 100159. https://doi.org/10.1016/j.mtsust.2022.100159

[36] G.L. Dotto, J.M.D. Moura, T.R.S. Cadaval, L.A.D.A. Pinto, Application of chitosan films for the removal of food dyes from aqueous solutions by adsorption, Chem. Engin. J. 214 (2013) 8–16. https://doi.org/10.1039/C4GC02483D.

[37] W.W. Ngah, L.C. Teong, M.A.K.M. Hanafiah, Adsorption of dyes and heavy metal ions by chitosan composites: A review, Carbohydr. Polym. 83 (2011) 1446–1456. https://doi.org/10.1016/j.carbpol.2010.11.004

[38] Z. Yu, C. Hu, A.B. Dichiara, W. Jiang, J. Gu, Cellulose Nanofibril/Carbon Nanomaterial Hybrid Aerogels for Adsorption Removal of Cationic and Anionic Organic Dyes, Nanomaterials 10 (2020) 169. https://doi.org/10.3390/nano10010169

[39] C. Li, X. Wang, D. Meng, L. Zhou, Facile synthesis of low-cost magnetic biosorbent from peach gum polysaccharide for selective and efficient removal of cationic dyes, Int. J. Biol. Macromol. 107 (2018) 1871e1878, https://doi.org/10.1016/j.ijbiomac.2017.10.058.

[40] S. Zeng, J. Long, J. Sun, G. Wang, L. Zhou, A review on peach gum polysaccharide: hydrolysis, structure, properties and applications, Carbohydr. Polym. 279 (2022) 119015, https://doi.org/10.1016/j.carbpol.2021.119015.

[41] Y. Song, Y. Duan, L. Zhou, Multi-carboxylic magnetic gel from hyperbranched polyglycerol formed by thiol-ene photopolymerization for efficient and selective adsorption of methylene blue and methyl violet dyes, J. Colloid Interface Sci. 529 (2018) 139e149, https://doi.org/10.1016/j.jcis.2018.06.005.

[42] H.A.M. Bacelo, S.C.R. Santos, C.M.S. Botelho, Tannin-based biosorbents for environmental applications – A review, Chem. Engin. J. 303 (2016) 575–587. https://doi.org/10.1016/j.cej.2016.06.044.

[43] Q. Ma, Y. Yu, M. Sindoro, A.G. Fane, R. Wang, H. Zhang, Carbon-Based Functional Materials Derived from Waste for Water Remediation and Energy Storage, Adv. Mater. 29 (2017) 1605361. https://doi.org/10.1002/adma.201605361

[44] P.X.T. Nguyen, K.H. Ho, N.H.N. Do, C.T.X. Nguyen, H.M. Nguyen, K.A. Tran, K.A. Le, P.K. Le, A comparative study on modification of aerogel-based biosorbents from coconut fibers for treatment of dye- and oil-contaminated water, Mater. Today Sustain. 19 (2022) 100175. https://doi.org/10.1016/j.mtsust.2022.100175

[45] H.C. Eisenman, A. Casadevall, Synthesis and assembly of fungal melanin, Appl Microbiol Biotechnol. 93 (2012) 931–940. https://doi.org/10.1007/s00253-011-3777-2

[46] R.V. Fogarty, J.M. Tobin, Fungal melanins and their interactions with metals, Enzyme and Microbial Technology 19, 4 (1996) 311-317. https://doi.org/10.1016/0141-0229(96)00002-6

[47] P. Jakubiak, F. Lack, J. Thun, A. Urtti, R. Alvarez-Sánchez, Influence of Melanin Characteristics on Drug Binding Properties, Mol. Pharmaceutics 16, 6 (2019) 2549–2556. https://doi.org/10.1021/acs.molpharmaceut.9b00157

[48] O. Karlsson, N.G. Lindquist, Melanin and neuromelanin binding of drugs and chemicals: toxicological implications, Arch Toxicol 90 (2016) 1883–1891. https://doi.org/10.1007/s00204-016-1757-0

[49] J.J. Oh, J.Y. Kim, Y.J. Kim, S. Kim, G.H. Kim, Utilization of extracellular fungal melanin as an eco-friendly biosorbent for treatment of metal-contaminated effluents, Chemosphere 272 (2021) 129884. https://doi.org/10.1016/j.chemosphere.2021.129884

[50] E. Priyadarshini, S.S. Priyadarshini, B.G. Cousins, N. Pradhan, Metal-Fungus interaction: Review on cellular processes underlying heavy metal detoxification and synthesis of metal nanoparticles, Chemosphere 274 (2021) 129976. https://doi.org/10.1016/j.chemosphere.2021.129976

[51] A.N. Tran-Ly, J. Ribera, F.W.M.R. Schwarze, M. Brunelli, G. Fortunato, Fungal melanin-based electrospun membranes for heavy metal detoxification of water, Sustainable Materials and Technologies 23 (2020) e00146. https://doi.org/10.1016/j.susmat.2019.e00146

[52] P. Manini, V. Lino, P. Franchi, G. Gentile, T. Sibillano, C. Giannini, E. Picardi, A. Napolitano, L. Valgimigli, C. Chiappe, M. d'Ischia, A Robust Fungal Allomelanin Mimic: An Antioxidant and Potent π-Electron Donor with Free-Radical Properties that can be Tuned by Ionic Liquids, ChemPlusChem 84 (2019) 1331-1337. https://doi.org/10.1002/cplu.201900195

[53] P. Manini, V. Lino, G. D'Errico, S. Reale, A. Napolitano, F. De Angelis, M. d'Ischia, "Blackness" is an index of redox complexity in melanin polymers, Polym. Chem. 11 (2020) 5005-5010. https://doi.org/10.1039/D0PY00700E

[54] P. Manini, V. Lucci, V. Lino, S. Sartini, F. Rossella, G. Falco, C. Chiappe, M. d'Ischia, Synthetic mycomelanin thin films as emergent bio-inspired interfaces controlling the fate of embryonic stem cells, J. Mater. Chem. B 8 (2020) 4412-4418. https://doi.org/10.1039/D0TB00623H

[55] H.M. Zhou, N.C. McCallum, Z.Y. Hu, W. Cao, K. Gnanasekaran, Y.N. Feng, J.F. Stoddart, Z. Wang, N.C. Gianneschi, Artificial Allomelanin Nanoparticles, ACS Nano 13 (2019) 10980−10990. https://doi.org/10.1021/acsnano.9b02160

[56] N.C. McCallum, F.A. Son, T.D. Clemons, S.J. Weigand, K. Gnanasekaran, C. Battistella, B.E. Barnes, H. Abeyratne-Perera, Z.E. Siwicka, C.J. Forman, X. Zhou, M.H. Moore, D.A. Savin, S.I. Stupp, Z. Wang, G.J. Vora, B.J. Johnson, O.K. Farha, N.C. Gianneschi, Allomelanin: A Biopolymer of Intrinsic Microporosity, J. Am. Chem. Soc. 143 (2021) 4005–4016. https://doi.org/10.1021/jacs.1c00748

[57] M. Rafatullah, O. Sulaiman, R. Hashim, A. Ahmad, Adsorption of methylene blue on low-cost adsorbents: a review, J. Haz. Mater. 177 (2010) 70-80. https://doi.org/10.1016/j.jhazmat.2009.12.047

[58] T. Robinson, G. McMullan, R. Marchant, P. Nigam, Remediation of Dyes in Textile Effluent: A Critical Review on Current Treatment Technologies with a Proposed Alternative, Bioresour. Technol. 77 (2001) 247−255. https://doi.org/10.1016/s0960-8524(00)00080-8

[59] A.A. Basaleh, M.H. Al-Malack, T.A. Saleh, Methylene Blue removal using polyamide-vermiculite nanocomposites: Kinetics, equilibrium and thermodynamic study, Journal of Environmental Chemical Engineering 7 (2019) 103107. https://doi.org/10.1016/j.jece.2019.103107.

[60] H. Chandarana, P.S. Kumar, M. Seenuvasan, M.A. Kumar, Kinetics, equilibrium and thermodynamic investigations of methylene blue dye removal using *Casuarina equisetifolia* pines, Chemosphere 285 (2021) 131480. https://doi.org/10.1016/j.chemosphere.2021.131480.

[61] J.Z. Guo, B. Li, L. Liu, K. Lv, Removal of methylene blue from aqueous solutions by chemically modified bamboo, Chemosphere 111 (2014) 225–231. https://doi.org/10.1016/j.chemosphere.2014.03.118

[62] U. Pal, A. Sandoval, S.I.U.M. Madrid, G. Corro, V. Sharma, P. Mohanty, Mixed titanium, silicon, and aluminum oxide nanostructures as novel adsorbent for removal of rhodamine 6G and methylene blue as cationic dyes from aqueous solution, Chemosphere 163 (2016) 142e152. https://doi.org/10.1016/j.chemosphere.2016.08.020

[63] H. Zeng, W. Qi, L. Zhai, F. Wang, J. Zhang, D. Li, Magnetic biochar synthesized with waterworks sludge and sewage sludge and its potential for methylene blue removal, Journal of Environmental Chemical Engineering 9 (2021) 105951. https://doi.org/10.1016/j.jece.2021.105951

[64] M.M. Cecchini, S. Reale, P. Manini, M. d'Ischia, F. De Angelis, Modeling Fungal Melanin Buildup: Biomimetic Polymerization of 1,8-Dihydroxynaphthalene Mapped by Mass Spectrometry, Chem. Eur. J. 23 (2017) 8092 – 8098. https://doi.org/10.1002/chem.201701951

[65] P. Manini, M. Bietti, M. Galeotti, M. Salamone, O. Lanzalunga, M.M. Cecchini, S. Reale, O. Crescenzi, A. Napolitano, F. De Angelis, V. Barone, M. d'Ischia, Characterization and Fate of Hydrogen-Bonded Free-Radical Intermediates and Their Coupling Products from the Hydrogen Atom Transfer Agent 1,8-Naphthalenediol. ACS Omega 3 (2018) 3918−3927. https://doi.org/10.1021/acsomega.8b00155

[66] A. Pezzella, M. Barra, A. Musto, A. Navarra, M. Alfè, P. Manini, S. Parisi, A. Cassinese, V. Criscuolo and M. d'Ischia, Stem cell-compatible eumelanin biointerface fabricated by chemically controlled solid state polymerization, Mater. Horiz. 2, (2015) 212–220. https://doi.org/10.1039/c4mh00097h

[67] E.P. Serjeant, B. Dempsey, International Union of Pure and Applied Chemistry. Commission on Equilibrium Data.; Ionisation constants of organic acids in aqueous solution. Oxford, New York, Pergamon Press, 1979.

[68] M.A. Mohammed, A. Shitu, A. Ibrahim, Removal of Methylene Blue Using Low Cost Adsorbent: A Review, Res. J. Chem. Sci. 4 (2014) 91-102.